

# Detecting Road Obstacles by Erasing Them \*

Krzysztof Lis   Sina Honari   Pascal Fua   Mathieu Salzmann

Computer Vision Laboratory, EPFL

## Abstract

Vehicles can encounter a myriad of obstacles on the road, and it is not feasible to record them all beforehand to train a detector. Our method selects image patches and inpaints them with the surrounding road texture, which tends to remove obstacles from those patches. It then uses a network trained to recognize discrepancies between the original patch and the inpainted one, which signals an erased obstacle.

We also contribute a new dataset for monocular road obstacle detection, and show that our approach outperforms the state-of-the-art methods on both our new dataset and the standard Fishyscapes Lost & Found benchmark.

## 1. Introduction

The vision-based obstacle detection system of a self-driving car should be able to handle all manners of potential hazards lying on the road. This includes people and animals, which are well represented in training databases, but also strange and unexpected objects that are not. Such objects are as rare as they are diverse, which makes the now standard approach of training deep networks by showing them an exhaustive set of annotated samples not directly applicable.

In practice, the difficulty of detecting arbitrary obstacles is thus often addressed using LiDAR sensors [31] or multiple cameras [27]. In this paper, we demonstrate that it can also be tackled using only a single RGB image. To this end, we rely on the fact that obstacles look different from the surrounding road surface. We can therefore detect them by inpainting image-patches from their surroundings and then checking how similar the inpainted patch is to the original one. While a similar intuition has been used to detect anomalies in



Figure 1. **Detecting unexpected obstacles.** **Top:** Three objects one would not expect to see on a road and that are not featured in standard databases. **Middle:** The road area has been inpainted. **Bottom:** After comparing the original and inpainted images, our discrepancy network returns a binary mask that denotes the obstacle locations.

several application scenarios, such as detecting manufacturing defects [37, 12] or anomalous faces [3], the very constrained nature of these tasks made it possible to rely on simple comparisons of handcrafted features. By contrast, on roads, this would yield many false positives due to road markings, diversity in road texture, and obstacles extending beyond the inpainted patch.

Our solution is to introduce a *discrepancy network* trained to recognize which differences between the inpainted patch and the original one are significant. It returns a per-pixel heatmap denoting the presence of obstacles. To train it to handle objects that are *not* part of the training database, we generate samples featuring synthetic obstacles by moving existing training objects, such as road signs and people, onto the road.

Our experiments show that our discrepancy network trained solely on Cityscapes [6] objects successfully detects obstacles on images depicting significantly dif-

\*This work was supported in part by the International Chair Drive for All - MINES ParisTech - Peugeot-Citroën - Safran - Valeo.

ferent road scenes, without requiring any annotated data nor any re-training for these new scenes. In other words, our method generalizes well to previously unseen real obstacles and new road surfaces. It outperforms earlier monocular road anomaly detectors [21, 4, 22, 2] on the *Lost & Found* [27] data featured in the *Fishyscapes* benchmark [4], as well as on our own newly collected dataset featuring additional unusual objects and road surfaces.

Our contribution is therefore a simple but effective approach to the detection of obstacles that never appeared in any training database, given only a single RGB image. We will make our obstacle detection code<sup>1</sup>, our semi-synthetic training dataset, and our new benchmark dataset<sup>2</sup> publicly available.

## 2. Related Work

In this section, we briefly review methods that, similar to ours, rely on a single RGB image for obstacle detection and do not use explicit obstacle training sets. For a more complete survey of obstacle detection algorithms, we refer the interested reader to [27, 28, 10, 35].

### 2.1. Image reconstruction for anomaly detection

If an image is reconstructed so as to preserve the appearance in normal regions and discard anomalous ones, those anomalies can be detected by comparing the input to the reconstruction. This has been achieved in several ways we now discuss.

The distribution of inlier images is represented by training an autoencoder in [1], followed by a feature comparison between the input and reconstruction. Auto-encoding has been used to find highway obstacles in [7, 25], where input patches are passed through a Restricted Boltzmann Machine. Its limited expressive power is supposed to preserve the smooth road surface while altering obstacles. This approach, however, does not address textured road surfaces. As opposed to encoding the input image, the method of [29] trains a generator to capture the training distribution and searches for a latent vector producing an image most similar to the input. This method operates on microscopic scans of tissue samples, however, to our knowledge, it has not been attempted with a distribution so diverse as outdoor road scenes.

Others [21, 34] explicitly restrict the intermediate representation of the scene to a dense semantic map, and synthesize a plausible matching image using conditional GANs for image translation [13, 33]. Since

the anomalous regions are not represented by the typical semantic classes, their appearance will be altered by this process. In [21], the input and synthesized images are compared using a learned discrepancy module, while [34] uses a feature distance measure.

Rather than encoding the input, one can remove parts of the image and inpaint them based on the surrounding context. In [12] square patches are inpainted and compared with an  $L_1$  metric to detect material defects; The method of [37] combines the reconstructions obtained with a set of random inpainting masks and uses a multi-scale gradient magnitude similarity metric for comparison. In the context of road scenes, [24] proposes to compare the road’s appearance to similar images memorized from previous video frames; however this would lead to false positives when entering an area with a new road texture. Furthermore, these methods assume high fidelity of the reconstruction, and detect every visible difference as an anomaly. In outdoor scenes with road markings and diverse surface textures, the inpainting is bound to be imperfect. We address this by training a discrepancy network to focus on the relevant differences.

### 2.2. Anomaly detection in semantic segmentation

The problem of detecting anomalies can be posed as one of open-set semantic segmentation. With standard, fully-supervised semantic segmentation networks, all pixels, including the anomalous ones will be classified into one of the training semantic categories. Open-set semantic segmentation then aims to find the outliers in the resulting semantic maps. The method of [2] introduces an outlier detection head sharing backbone features with the semantic segmentation head. It is trained using extensive out-of-distribution data, injecting outlier patches drawn from ImageNet-1k [8] into the Cityscapes and Vistas [26] scenes.

The work of [4] proposes to learn the inlier distribution of features extracted from a layer of the semantic segmentation network. It uses a normalizing flow to bijectively map the features to latent vectors following a Gaussian distribution. The mapping is trained to maximize the likelihood of the features observed in inlier samples.

Another approach consists of estimating the uncertainty of label prediction based on the assumption that outlier regions should yield low classification confidence. Bayesian deep learning considers the network weights and outputs to be probability distributions. In practice, dropout [32] is used to approximate the distribution over model weights, applied to semantic segmentation in [14, 15]. Alternatively an ensemble of networks can be used [18, 11]. In [22], the Dirichlet dif-

<sup>1</sup> Code and semi-synthetic training set:  
[github.com/cvlab-epfl/erasing-road-obstacles](https://github.com/cvlab-epfl/erasing-road-obstacles)

<sup>2</sup> Road Obstacles dataset:  
[www.epfl.ch/labs/cvlab/data/road-obstacles-2020](http://www.epfl.ch/labs/cvlab/data/road-obstacles-2020)

ferential entropy is used as a measure of uncertainty. We find that the performance of those methods as obstacle detectors degrades significantly when faced with road surfaces differing from the training set, as apparently the novel textures are treated as anomalies. We will show that our approach based on comparing the original image with an inpainted one with a discrepancy detector does not suffer from this drawback.

### 3. Approach

Our goal is to identify obstacles that are on the road because those are the ones that truly matter for autonomous driving. In this work, we will therefore focus on the road, whose location we assume to be known *a priori*. This is a realistic assumption given that most self-driving algorithms include a road- or lane-detection algorithm such as a semantic segmentation network of [38] trained on the Cityscapes dataset [6], which is the one we use in practice. Given the road area in the image, our goal is to identify all image pixels within it that belong to obstacles.

The difficulty is that the obstacle objects can be observed in many forms. Furthermore, because they are unexpected, there is no guarantee that they were present in the training database to train the network to recognize them.

Hence, the network must be taught to capture the generic idea of “an object that does not belong on the road”.

To this end, given a binary mask denoting the drivable area in the image, we propose the following two-step approach:

1. Erase the obstacles by removing road patches and inpaint them in a sliding-window manner;
2. Use a discrepancy network to compare the original image to the inpainted one and decide if they are similar enough.

The intuition behind this approach is that, if there is an obstacle, the inpainted area will look very different from the original image. However, even if there is no obstacle, the inpainted area will be similar to the original one, but not strictly equal. Hence, the discrepancy network is needed to assess if they are dissimilar enough to flag a potential obstacle. This yields a heatmap denoting the likelihood of each pixel in the drivable area belonging to an obstacle. In the remainder of this section, we discuss these two steps in more detail.

#### 3.1. Inpainting

To erase the obstacles while preserving the surrounding road appearance, we use a general-purpose

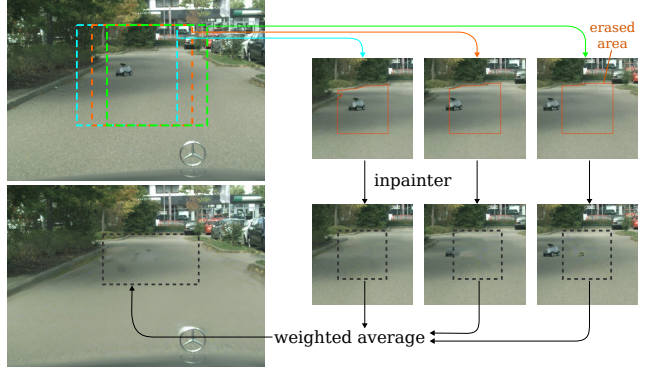


Figure 2. **Sliding window inpainting of the road surface.** We extract  $400 \times 400$  context patches then erase and inpaint the road area contained within the central  $200 \times 200$  of the patch. Finally we fuse the inpaintings which reconstructs the road appearance while removing localized obstacles. Note how the process was able to preserve the shadow of the trees.

inpainter [36] that relies on an adversarial approach to ensure that the inpainted image looks realistic. We use a version of their model trained on the scene recognition dataset Places2 [39], and do not train it further.

A naive way to use it would be to inpaint the entire road area at once. This, however, would provide no indication to the inpainter of the road appearance, leading to inpainted images that differ from the original ones in the whole road region, thus precluding subsequent obstacle detection.

Instead, we inpaint road patches to provide sufficient context for the network to reconstruct the road surface, as shown in Fig. 2. The patches nonetheless need to be large enough to encompass obstacles whose size we do not know *a priori*. We therefore follow a sliding-window approach, inpainting patches of  $200 \times 200$  pixels of drivable area within  $400 \times 400$  image regions to provide context.

While an obstacle is usually nicely erased when the area to inpaint encloses it completely, the inpainter is able to re-create the obstacles that are only partially contained in the inpainted region. To resolve this, we use consecutive patches with a relative overlap of 0.7, increasing the likelihood of having at least one patch that covers the entire obstacle. This means that each image pixel is inpainted multiple times. We then fuse the multiple inpaintings of each pixel by weighted averaging, where the weight of each inpainting is computed based on the Manhattan distance between the corresponding patch center and the pixel location of interest. Formally, a patch centered at location  $\mathbf{c}_j = [u_j, v_j]^\top$  contributes to the inpainting of a pixel at location

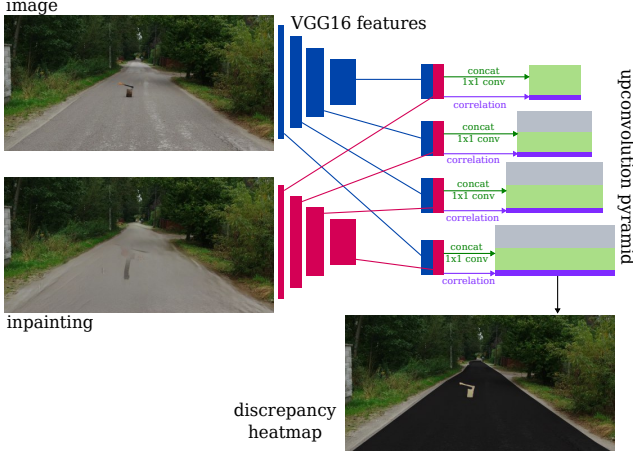


Figure 3. **Architecture of the discrepancy network**

$\mathbf{p} = [u, v]^\top$  with a weight

$$w = \frac{1 - \frac{2}{s} \max(|u - u_j|, |v - v_j|)}{\sum_{[u_i, v_i] \in \Pi(u, v)} 1 - \frac{2}{s} \max(|u - u_i|, |v - v_i|)}, \quad (1)$$

where  $s$  is the patch width or height and  $\Pi(u, v)$  is the set of patches overlapping the  $[u, v]^\top$  pixel, with each patch having a center at  $[u_i, v_i]$ .

### 3.2. Discrepancy Network

While our inpainting strategy preserves the general appearance of the road surface, it still yields unavoidable imperfections due to road markings, texture details, and the non-zero contributions of obstacles located close to the patch edges. Thus, simply comparing the original image with the inpainted one via pixel difference would yield many false positive detections. To handle this, we introduce a *discrepancy network* that we train to distinguish significant differences from inpainting artifacts.

We implement our discrepancy network using a two-stream architecture, shown in Fig. 3, that takes as input the original image and the inpainted one. Both inputs are first processed by a VGG [30] feature extractor. The resulting features are then concatenated and fused through  $1 \times 1$  convolutions. Furthermore, we compute a point-wise correlation map of the image and inpainting features, which we append as an additional channel to the output of the  $1 \times 1$  convolutions. The concatenated features are then passed to the upconvolution pyramid. Finally, we obtain the desired heatmap via an up-convolution pyramid followed by a softmax.

#### 3.2.1 Training the Discrepancy Network

Recall that we target unusual road obstacles that may never have been seen at training time. There-

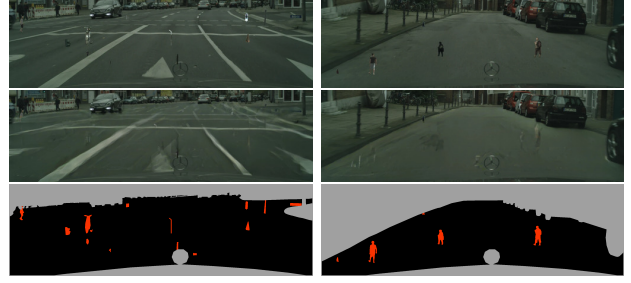


Figure 4. **Synthetic training obstacles.** Using the Cityscapes dataset, we transplant random object instances onto the road to appear as small obstacles (top). Results of the inpainting process (middle). Labels (bottom): the discrepancy network is trained to distinguish obstacles (red) from the road area (black), while the background grey region is ignored in training.



Figure 5. **Incorporating noise.** We augment the training images (left) by adding noise summed at two scales and magnitudes (right) to simulate a diverse road texture and prevent the discrepancy network from becoming excessively sensitive to high frequencies.

fore, we need the discrepancy network to generalize to previously-unseen objects.

To tackle this challenge, we built a synthetic training set from only the Cityscapes [6] dataset, which contains no unusual traffic obstacles. We extracted instances of people and vehicles using the instance annotations, together with *traffic lights* and *traffic signs*, which lack instance labels, but can be extracted as connected components within their pixel-wise semantic label mask. Since many road obstacles are small and difficult to detect, to simulate small obstacles seen from a far distance, we selected from the whole dataset instances of size ranging from 10 to 150 pixels, and area between 100 and 5000 pixel squared. We then sampled random objects from this database and overlaid them onto the drivable area to mimic obstacles. Fig. 4 features several images synthesized in this way.

#### 3.2.2 High-frequency Appearance Variations

Our approach to overlaying synthetic obstacles on real roads introduces sharp discontinuities in our training images. This makes the discrepancy network over-



sensitive to high-frequency appearance variations, leading to false positives in test images depicting road surfaces rougher than the Cityscapes ones. We address this issue by first applying a Gaussian blur to the training images and then adding noise of two different scales to them in order to create a more realistic texture, as shown in Fig. 5. We also blur the input images at test time. We will evaluate the influence of the blur kernel size in our experiments in Section 4.5. We do not blur the inpainted image since our patch fusion strategy already tends to smoothe it.

## 4. Experiments

In this section, we first present the baselines, evaluation metrics, and datasets used in our experiments. We then compare our approach to the baselines and finally perform an ablation study.

### 4.1. Baselines

**Resynthesis.** The method of [21] performs semantic segmentation of the image and then synthesizes an image solely from the resulting semantic map using a conditional GAN [33]. Since the anomalous regions are not represented by any of the predefined semantic classes, their reconstructed appearance will differ significantly from the original image. These differences are detected by a discrepancy network similar in purpose to the one we use, which is trained by synthetically swapping object classes in Cityscapes.

**Discriminative Outlier Detection Head [2].** This method relies on an outlier detection head that shares backbone features with a semantic segmentation head. The resulting two-head network is trained using frames from Cityscapes and Vistas [26], with injected outliers drawn from ImageNet-1k [8]. We evaluate a variant that uses constant-size outliers, one where their size is randomized, and one combining the outputs of the previous two.

The following methods are described in detail in the Fishyscapes benchmark [4]. They are all built around a DeepLab [5] semantic segmentation network trained on Cityscapes. They aim to learn the distribution of the training images and detect image regions falling outside that distribution.

**Learned Embedding Density [4].** It learns the inlier distribution of features extracted from a layer of the DeepLab [5] network. It uses a normalizing flow to bijectively map the features to latent vectors following a Gaussian distribution. The mapping is trained to maximize the likelihood of the features observed in inlier samples.

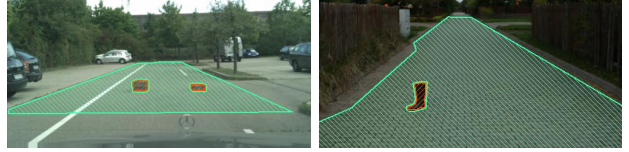


Figure 6. **Example ground-truth labels.** We consider the task of distinguishing obstacle pixels (orange) from the road area (light green), while the background (not marked) is excluded from the evaluation.

**DeepLab Softmax Entropy [19].** It measures the entropy of the class likelihoods produced by the final softmax layer of the DeepLab semantic segmentation network.

**OoD Training [19].** This approach uses the Cityscapes *void* areas as examples of outliers. It can then either explicitly add *void* to the set of predicted classes, or learn to maximize the softmax entropy in the *void* regions.

**Bayesian DeepLab [23].** This model introduces dropout layers into the DeepLab network. At inference time, it draws samples by randomizing the dropout. The uncertainty is measured as the mutual information between the resulting distribution and the network weights.

**Dirichlet DeepLab [22].** This approach outputs the  $\alpha$  parameters defining a Dirichlet distribution over the class labels, rather than a single set of class likelihoods given by the softmax. The network is trained to produce sharp distributions for inlier classes and a uniform distribution for the *void* class. The anomaly score is calculated as the Dirichlet differential entropy.

### 4.2. Evaluation Metrics

Since we focus on detecting obstacles on the road, we take the Region of Interest (ROI) to be the ground-truth road area as shown in Fig. 6. We formulate our task in terms of pixel-wise binary classification. Our method, like the baselines we compare with, outputs a heatmap in the range from 0 to 1 denoting the likelihood of each pixel within the ROI to belong to an obstacle. We use the following two metrics of the *Fishyscapes* benchmark [4]:

- The primary metric is Average Precision (AP), that is, the area under the precision-recall curve. This metric is more meaningful than metrics based on the receiver operating curve (ROC) due to strong class imbalance, as obstacles typically cover less than 2% of the total road surface.
- A secondary metric is false positive rate (FPR) at a 95% true positive rate (TPR), which we denote

### 4.3. Datasets

**Fishyscapes Lost & Found.** The Lost & Found dataset [27] contains image sequences captured by a vehicle approaching lost cargo items placed on parking lots and streets. A subset of 100 frames was selected for the Fishyscapes [4] benchmark of anomaly detection in road scenes to avoid non-anomalous Cityscapes objects, such as people. We adapt the benchmark to the task of obstacle detection on known road regions by restricting the evaluation to the ground-truth labeled drivable area. This was achieved in collaboration with the Fishyscapes benchmark organizers, who will integrate this evaluation strategy in the benchmark.

It features six different scenes. We collected 5 images in one scene and 20 images in each one of other 5 scenes, making a total of 105 labeled  $2048 \times 1024$  frames. The labels include pixel masks for individual obstacle instances along with approximate outlines of the drivable area. We take the ROI to be the area within these outlines. If an object has a hole, such as a basket with a handle, we label the hole as outside of the ROI and ignore it in our evaluations, as we do for the background.

#### 4.4. Comparative Results

Our method clearly outperforms all others in terms Average Precision (AP), the primary metric in [4]. The only other method that performs consistently well on both datasets is the Discriminative Outlier Detection Head [2]. However, it requires extensive out-of-distribution ImageNet data for training whereas we only use Cityscapes, which contains no unusual objects.

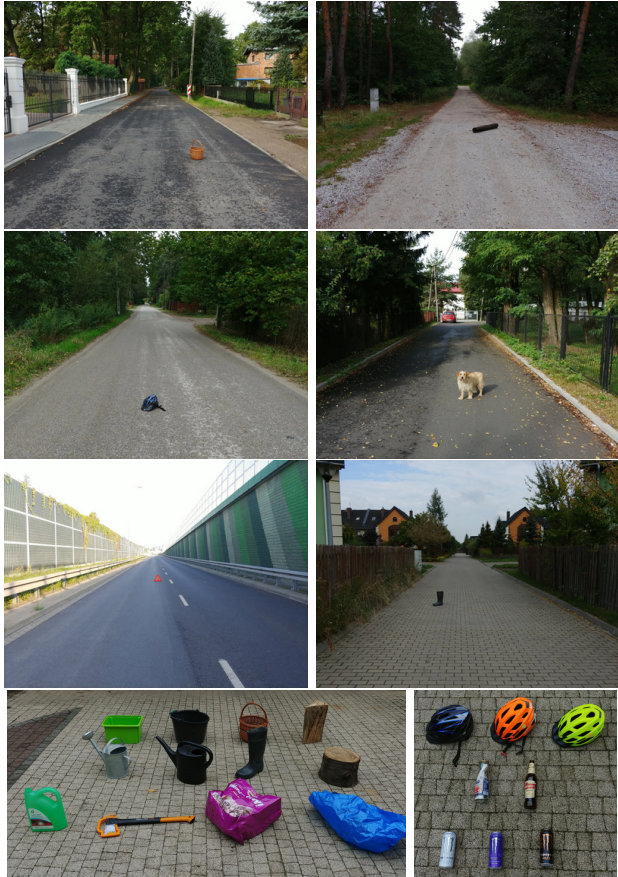


Figure 7. **Road Obstacles dataset.** Top: Example frames representing each of the 6 scenes. Bottom: Some of the objects featured in the dataset.

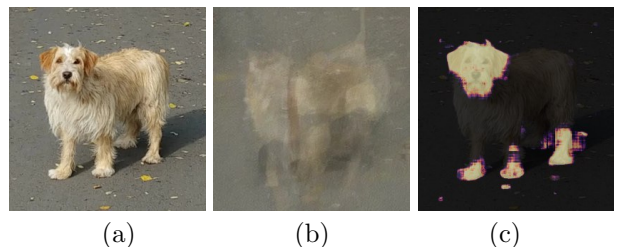


Figure 8. **Failure Mode on Large Objects.** (a) A nearby dog is significantly larger than our training examples and overlaps the boundaries of the inpainted patches. (b) Hence, it is not erased effectively. (c) Our method, trained on smaller objects, detects parts of the dog as separate obstacles. Nevertheless, this would be enough to alert a self-driving system of the presence of an obstacle.

Our result on the False Positive Rate at 95% True Positive Rate (FPR<sub>95</sub>) compares well to most of methods, except Resynthesis [21] that delivers better results on both datasets and one variant of Discriminative Outlier Discriminative Head [2] that prevails on *Road Obstacles*. Note, however, that the latter variant does

Method		Fishyscapes: Lost & Found		Road Obstacles	
		AP $\uparrow$	FPR <sub>95</sub> $\downarrow$	AP $\uparrow$	FPR <sub>95</sub> $\downarrow$
Ours	discrepancy network	<b>81.0</b>	9.1	<b>75.9</b>	15.8
Discriminative Outlier Detection Head [2]	combined probability	68.3	10.7	68.1	19.1
	random sized patches	60.9	27.0	70.6	<b>1.0</b>
	fixed sized patches	50.0	73.9	31.4	28.1
Resynthesis [21]	discrepancy network	65.4	<b>6.9</b>	43.7	2.3
Dirichlet DeepLab [22]	prior entropy	61.1	70.8	10.7	22.8
Learned Embedding Density [4]	minimum NLL	60.3	8.5	2.1	31.3
	logistic regression	55.3	9.0	1.8	33.9
	single-layer NLL	47.5	17.3	-	-
Bayesian DeepLab [23]	entropy	53.7	37.3	-	-
	mutual information	43.6	34.0	8.2	57.9
DeepLab Softmax [19]	entropy	29.2	41.0	16.1	9.1
kNN Embedding	density	21.8	20.9	-	-
	relative class density	6.9	100.0	-	-
OoD training	void classifier	14.9	24.2	9.3	48.8
	max-entropy	13.6	14.1	2.4	11.6

Table 1. **Obstacle detection scores.** The primary metric is *average precision* of detecting obstacle pixels.

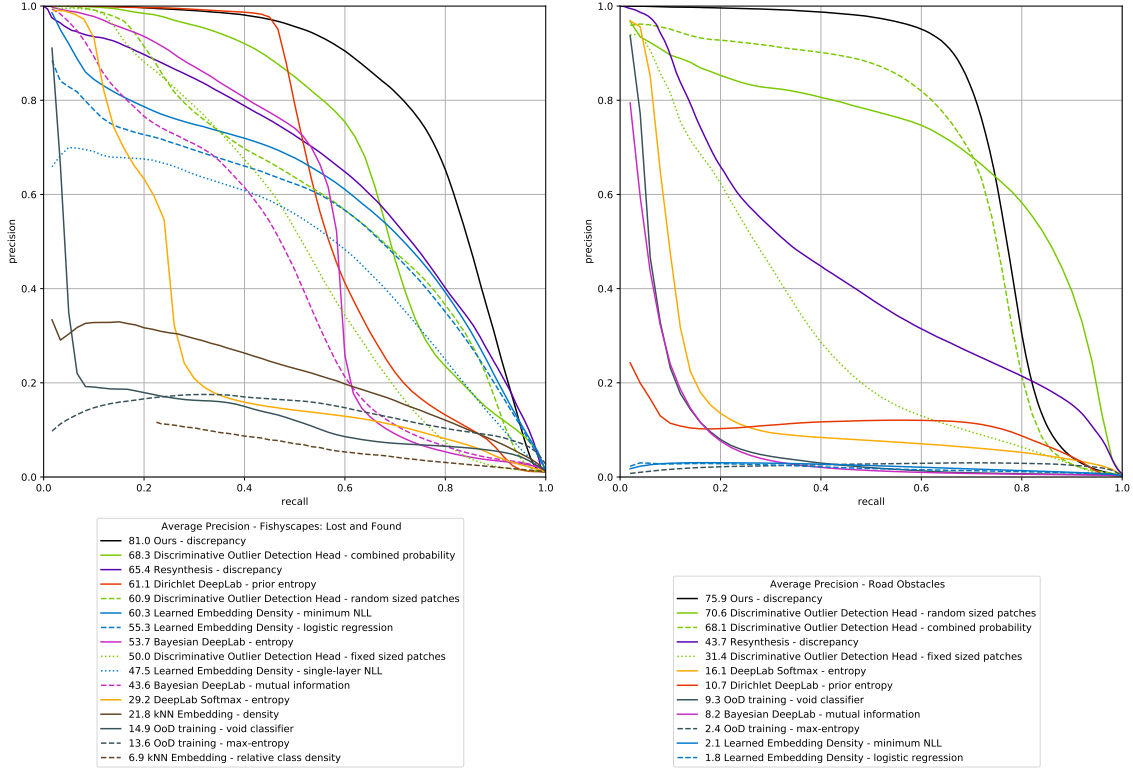


Figure 9. **Obstacle detection Precision-Recall curves.**

poorly on the other dataset. Careful examination of our results reveals we could easily improve our FPR<sub>95</sub> performance by accounting more carefully for large objects: Our training set contains only instances smaller than 5000 pixels squared, with the median area being 820. Hence, when encountering significantly larger objects, our network detects parts of them and omits the

internal regions, as shown in Fig. 8. To confirm this, we simply removed the 4 frames out of 105 Road Obstacles frames containing obstacles exceeding 10,000 pixels in size and our FPR<sub>95</sub> score improved from 15.8% to 0.7%. Conversely, re-running Resynthesis on the modified dataset increased the FPR<sub>95</sub> from 2.3% to 2.5%.

In any event, even though breaking up big objects



Method	Fishyscapes: Lost & Found		Road Obstacles	
	AP $\uparrow$	FPR <sub>95</sub> $\downarrow$	AP $\uparrow$	FPR <sub>95</sub> $\downarrow$
Image vs Inpainting + noise augmentation	<b>81.0</b>	<b>9.1</b>	<b>75.9</b>	<b>15.8</b>
Image vs Inpainting	78.8	18.0	72.3	42.6
Image vs Resynthesis + noise augmentation	79.6	30.1	71.8	43.0
Single image only	79.2	16.4	71.1	46.9
Single image only + noise augmentation	79.9	19.6	69.8	48.8
$L_1$ distance between image and inpainting	19.7	49.6	13.6	43.4

Table 2. **Ablation study results.** The variants are ordered by their performance on the *Road Obstacles* dataset - the inpainting method is better able to adapt to its diverse road surfaces. *Single-image* and *GAN Resynthesis* work well in Lost & Found whose roads resemble the Cityscapes training data.

	Training					
	no blur		3		5	
Inference	L&F	RO	L&F	RO	L&F	RO
no blur	<b>78.9</b>	76.2	65.0	12.0	55.8	8.4
3	77.5	<b>76.7</b>	<u>82.1</u>	69.6	79.3	49.9
5	75.4	73.1	81.0	<b>75.9</b>	<b>80.0</b>	68.4
7	71.7	68.1	78.2	74.3	77.8	<b>74.4</b>

Table 3. **Influence of the Gaussian blur.** We report the average precision as a function of the kernel size of the Gaussian blur applied to input images during training and inference. L&F and RO denote the *Fishyscapes Lost & Found* and *Road Obstacles* datasets, respectively. We choose a  $3 \times 3$  blur for training and a  $5 \times 5$  one for inference, combining stability and good performance. The bolded value shows the best performance in each setting, while the underline indicates the best performance in all settings.

into smaller ones degrades our FPR<sub>95</sub> performance, it would be sufficient to alert a self-driving system to the presence of obstacles. In future work, we will address this issue by using the scene layout to vary the inpainting window size according to the distance to the vehicle and will extend the training set with larger nearby objects.

#### 4.5. Ablation study

Table 2 shows the results of an ablation study where the discrepancy network was retrained with selected components altered or disabled.

In the *Image vs Resynthesis* variant, the inpainting described in Section 3.1 is replaced by an image synthesizer [33] from predicted semantic labels as in [21]. While the inpainter can reconstruct novel road textures based on the visual context, the generator produces a texture similar to the training roads, and this is reflected by degraded performance on *Road Obstacles*.

The *Single image only* variant uses only the monocular input image and no inpainting. We keep the architecture unchanged, but pass two copies of the image into both input streams. This also degrades perfor-

mance, confirming the importance of inpainting. We can also do the opposite, remove the discrepancy network, and compute the  $L_1$  distance between the RGB values of the input image and the inpainted result. The results are even worse, this time confirming how important the discrepancy network is. The addition of noise to training images, described in Section 3.2.2, prevents overfitting to smooth training road surfaces.

In Table 3, we further study the impact of the kernel size we use when blurring the image passed to the discrepancy network. We observe the best performance when the blur at inference is slightly stronger than at training. We use a kernel of size  $3 \times 3$  during training and  $5 \times 5$  at inference.

## 5. Conclusion

We have introduced a pipeline capable of detecting road obstacles in driving scenarios, given only single monocular images as input. We perform inpainting of the drivable area, erasing the localized obstacles while preserving the road surface. Our discrepancy network learns to accurately detect the removed obstacles and ignore irrelevant artifacts of reconstruction. This detector, trained only with synthetically altered Cityscapes data, is capable of generalizing to a variety of real-world obstacles and road surfaces. We have demonstrated this on *Fishyscapes Lost & Found* benchmark as well as our newly collected dataset. We will release our dataset to the community to help researchers in this field. In the future, we plan to exploit adaptive inpainting patch sizes and improve the fusion algorithm to address a wider range of obstacle dimensions.

## Acknowledgements

We thank Hermann Blum for adapting the Fishyscapes benchmark and baseline methods to our data.

We thank Mirosław Lis for assistance in the collection of the *Road Obstacles* dataset.



## References

- [1] S. Akcay, A. Atapour-Abarghouei, and T. P. Breckon. Ganomaly: Semi-Supervised Anomaly Detection via Adversarial Training. In *Asian Conference on Computer Vision*, 2018. 2
- [2] P. Bevandić, I. Krešo, M. Oršić, and S. Šegvić. Simultaneous Semantic Segmentation and Outlier Detection in Presence of Domain Shift. In *German Conference on Pattern Recognition*, 2019. 2, 5, 6, 7, 12
- [3] A. Bhattad, J. Rock, and D. Forsyth. Detecting Anomalous Faces with ‘No Peeking’ Autoencoders. In *Conference on Computer Vision and Pattern Recognition*, 2018. 1
- [4] H. Blum, P.-E. Sarlin, J. Nieto, R. Siegwart, and C. Cadena. Fishyscapes: A Benchmark for Safe Semantic Segmentation in Autonomous Driving. In *International Conference on Computer Vision*, October 2019. 2, 5, 6, 7, 12
- [5] L. Chen, G. Papandreou, I. Kokkinos, K. Murphy, and A. L. Yuille. Deeplab: Semantic Image Segmentation with Deep Convolutional Nets, Atrous Convolution, and Fully Connected CRFs. *IEEE Transactions on Pattern Analysis and Machine Intelligence*, 2018. 5
- [6] M. Cordts, M. Omran, S. Ramos, T. Rehfeld, M. Enzweiler, R. Benenson, U. Franke, S. Roth, and B. Schiele. The Cityscapes Dataset for Semantic Urban Scene Understanding. In *Conference on Computer Vision and Pattern Recognition*, 2016. 1, 3, 4, 12
- [7] C. Creusot and A. Munawar. Real-Time Small Obstacle Detection on Highways Using Compressive RBM Road Reconstruction. In *Intelligent Vehicles Symposium*, 2015. 2
- [8] J. Deng, W. Dong, R. Socher, L.-J. Li, K. Li, and L. Fei-Fei. Imagenet: A Large-Scale Hierarchical Image Database. In *Conference on Computer Vision and Pattern Recognition*, 2009. 2, 5
- [9] Jian Guo, He He, Tong He, Leonard Lausen, Mu Li, Haibin Lin, Xingjian Shi, Chenguang Wang, Junyuan Xie, Sheng Zha, Aston Zhang, Hang Zhang, Zhi Zhang, Zhongyue Zhang, Shuai Zheng, and Yi Zhu. Gluoncv and gluonnlp: Deep learning in computer vision and natural language processing. *Journal of Machine Learning Research*, 21(23):1–7, 2020. 12
- [10] Krishnam Gupta, Syed Ashar Javed, Vineet Gandhi, and K Madhava Krishna. MergeNet: A Deep Net Architecture for Small Obstacle Discovery. In *International Conference on Robotics and Automation*, 2018. 2
- [11] F. K. Gustafsson, M. Danelljan, and T. B. Schön. Evaluating Scalable Bayesian Deep Learning Methods for Robust Computer Vision. In *Conference on Computer Vision and Pattern Recognition*, 2020. 2
- [12] M. Haselmann, D. P. Gruber, and P. Tabatabai. Anomaly Detection Using Deep Learning Based Image Completion. In *International Conference on Machine Learning*, 2018. 1, 2
- [13] P. Isola, J. Zhu, T. Zhou, and A. Efros. Image-To-Image Translation with Conditional Adversarial Networks. In *arXiv Preprint*, 2016. 2
- [14] A. Kendall, V. Badrinarayanan, and R. Cipolla. Bayesian Segnet: Model Uncertainty in Deep Convolutional Encoder-Decoder Architectures for Scene Understanding. In *arXiv Preprint*, 2015. 2
- [15] A. Kendall and Y. Gal. What Uncertainties Do We Need in Bayesian Deep Learning for Computer Vision? In *Advances in Neural Information Processing Systems*, 2017. 2
- [16] D. P. Kingma and J. Ba. Adam: A Method for Stochastic Optimisation. In *International Conference on Learning Representations*, 2015. 12
- [17] G. Klambauer, T. Unterthiner, A. Mayr, and S. Hochreiter. Self-Normalizing Neural Networks. In *Advances in Neural Information Processing Systems*, 2017. 12
- [18] B. Lakshminarayanan, A. Pritzel, and C. Blundell. Simple and Scalable Predictive Uncertainty Estimation Using Deep Ensembles. In *Advances in Neural Information Processing Systems*, 2017. 2
- [19] K. Lee, H. Lee, K. Lee, and J. Shin. Training Confidence-Calibrated Classifiers for Detecting Out-Of-Distribution Samples. In *International Conference on Learning Representations*, 2018. 5, 7, 12
- [20] W. Li, O. H. Jafari, and C. Rother. Deep Object Co-Segmentation. In *Asian Conference on Computer Vision*, 2018. 12
- [21] K. Lis, K. Nakka, M. Salzmann, and P. Fua. Detecting the Unexpected via Image Resynthesis. In *International Conference on Computer Vision*, 2019. 2, 5, 6, 7, 8, 11, 12, 17
- [22] A. Malinin and M. Gales. Predictive Uncertainty Estimation via Prior Networks. In S. Bengio, H. Wallach, H. Larochelle, K. Grauman, N. Cesa-Bianchi, and R. Garnett, editors, *Advances in Neural Information Processing Systems*. 2018. 2, 5, 7, 12
- [23] J. Mukhoti and Y. Gal. Evaluating Bayesian Deep Learning Methods for Semantic Segmentation. In *arXiv Preprint*, 2018. 5, 7, 12
- [24] A. Munawar and C. Creusot. Structural Inpainting of Road Patches for Anomaly Detection. In *IAPR International Conference on Machine Vision Applications*, 2015. 2
- [25] A. Munawar, P. Vinayavekhin, and G. De Magistris. Limiting the Reconstruction Capability of Generative Neural Network Using Negative Learning. In *IEEE International Workshop on Machine Learning for Signal Processing*, 2017. 2
- [26] Gerhard Neuhold, Tobias Ollmann, Samuel Rota Buló, and Peter Kotschieder. The Mapillary Vistas Dataset for Semantic Understanding of Street Scenes. In *Conference on Computer Vision and Pattern Recognition*, 2017. 2, 5
- [27] P. Pinggera, S. Ramos, S. Gehrig, U. Franke, C. Rother, and R. Mester. Lost and Found: Detecting

- Small Road Hazards for Self-Driving Vehicles. In *International Conference on Intelligent Robots and Systems*, 2016. 1, 2, 6
- [28] S. Ramos, S. Gehrig, P. Pinggera, U. Franke, and C. Rother. Detecting Unexpected Obstacles for Self-Driving Cars: Fusing Deep Learning and Geometric Modeling. In *IEEE Intelligent Vehicles Symposium*, 2017. 2
- [29] T. Schlegl, P. Seeböck, S. M. Waldstein, U. Schmidt-Erfurth, and G. Langs. Unsupervised Anomaly Detection with Generative Adversarial Networks to Guide Marker Discovery. In *International Conference on Information Processing in Medical Imaging*, 2017. 2
- [30] K. Simonyan and A. Zisserman. Very Deep Convolutional Networks for Large-Scale Image Recognition. In *International Conference on Learning Representations*, 2015. 4, 12
- [31] Aasheesh Singh, Aditya Kamireddypalli, Vineet Gandhi, and K Madhava Krishna. LiDAR guided Small obstacle Segmentation. *arXiv preprint arXiv:2003.05970*, 2020. 1
- [32] N. Srivastava, G. Hinton, A. Krizhevsky, I. Sutskever, and R. Salakhutdinov. Dropout: A Simple Way to Prevent Neural Networks from Overfitting. *Journal of Machine Learning Research*, 15:1929–1958, 2014. 2
- [33] T.-C. Wang, M.-Y. Liu, J.-Y. Zhu, A. Tao, J. Kautz, and B. Catanzaro. High-Resolution Image Synthesis and Semantic Manipulation with Conditional GANs. In *Conference on Computer Vision and Pattern Recognition*, 2018. 2, 5, 8
- [34] Y. Xia, Y. Zhang, F. Liu, W. Shen, and A. Yuille. Synthesize Then Compare: Detecting Failures and Anomalies for Semantic Segmentation. In *European Conference on Computer Vision*, 2020. 2
- [35] F. Xue, A. Ming, M. Zhou, and Y. Zhou. A Novel Multi-Layer Framework for Tiny Obstacle Discovery. In *International Conference on Robotics and Automation*, 2019. 2
- [36] J. Yu, Z. Lin, J. Yang, X. Shen, X. Lu, and T. S. Huang. Free-Form Image Inpainting with Gated Convolution. In *Conference on Computer Vision and Pattern Recognition*, 2019. 3
- [37] V. Zavrtanik, M. Kristan, and D. Skoaj. Reconstruction by Inpainting for Visual Anomaly Detection. *Pattern Recognition*, 2020. 1, 2
- [38] H. Zhao, J. Shi, X. Qi, X. Wang, and J. Jia. Pyramid Scene Parsing Network. In *Conference on Computer Vision and Pattern Recognition*, 2017. 3, 11, 12
- [39] B. Zhou, A. Lapedriza, A. Khosla, A. Oliva, and A. Torralba. Places: A 10 Million Image Database for Scene Recognition. *IEEE Transactions on Pattern Analysis and Machine Intelligence*, 2017. 3

# Supplement

## A. Qualitative Results and Obstacle Size

Fig. 11 and Fig. 12 depict our results qualitatively. Our method does well on small obstacles but, as noted in Section 4.4 of the main paper, our  $FPR_{95}$  results are negatively impacted by the fact that we only trained with obstacles of size smaller than 5000 pixels squared. We made this choice to focus on obstacles seen at a distance, which are the ones that are crucial from a self-driving perspective: Once an obstacle is very large in the field of view, it usually is already too late to brake.

To demonstrate this, we perform binary classification by thresholding the obstacle heatmap, and plot how the true positive and false negative pixels are distributed among obstacles in Fig. 14. We set the threshold to 0.1 out of the 0.0 to 1.0 output range, because at this level the *recall* of both methods is similar; at higher thresholds, the recall of Resynthesis falls quickly, which is consistent with its low *average precision* score. Of course this low threshold leads to many false positives, so it is not suitable for real applications. Our method achieves high recall for the small obstacles, but lower recall for the large ones. Those obstacles are still partially detected, so a driving system would be aware of them, but not all of their pixels are marked. By contrast, the Resynthesis [21] method covers a larger area of the big obstacles, but misses some of the smaller obstacles completely, which is unsafe for a driving systems that needs to detect all objects. In Resynthesis, the obstacles with large areas have an out-sized influence over per-pixel metrics such as  $FPR_{95}$ , granting Resynthesis a better score than that of our method, despite its failure to detect several small objects. Hence,  $FPR_{95}$  may not be the most significant measures for these kinds of applications.

Furthermore, if  $FPR_{95}$  truly were the metric we care about, there is a simple way to improve it, that is, introduce larger objects in the training database, as follows.

To generate the synthetic data presented in this paper, we first extract all objects from Cityscapes annotations and filter them by dimension and area and then use them as synthetic obstacles. To study the impact of using larger objects, we generated a "big object" variant of our training set:

- In the version presented in the main paper, the filter selects instances with width and height between 10 and 150 pixels, and area between 100 and 5000 pixels squared, resulting in 61582 selected objects.

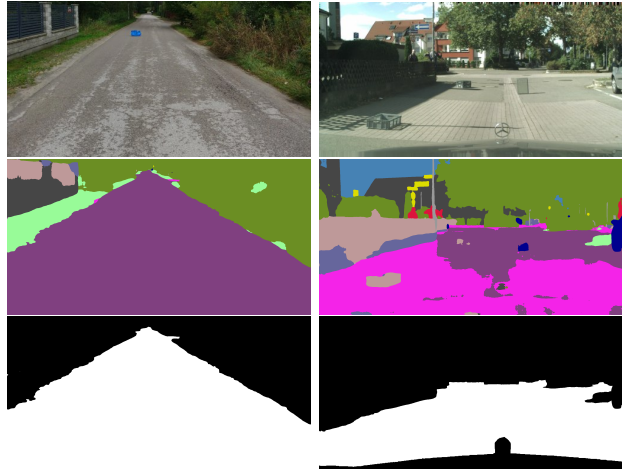


Figure 10. **Drivable space from semantic segmentation.** **Top:** Input images. **Middle:** Semantic segmentation performed by PSP-Net [38], the class colors follow Cityscapes convention. **Bottom:** We take the drivable space to be the union of *road* (purple) and *sidewalk* (magenta) pixels. The parts of obstacles can sometimes be classified as non-road, so we include the regions of other classes fully enclosed within the road area. In *Lost & Found*, the known ego-vehicle mask is excluded.

- In the *big object* variant, the filter selects instances with width and height between 10 and 250 pixels, and area between 100 and 35000 pixels squared, resulting in 77617 selected objects.

This simple change strongly boosts our method’s performance, as shown in Table 4. It significantly improves the  $FPR_{95}$  metric on both dataset, and increases the average precision too. The *big object* variant of our method now clearly outperforms all competing methods on *both* metrics in *Lost & Found* dataset as well as on AP in Road Obstacles dataset, while the  $FPR_{95}$  is also much lower compared to the variant trained with standard object sizes reported in the main paper. This demonstrates the significance of object size in training. In future work we perform a detailed investigation of ways to better handle the size variation of the obstacles, such as resizing the training objects or scale augmentation during training.

## B. Implementation details

In this section, we present details on drivable area selection and discrepancy network architecture and training.

### B.1. Determining the drivable area

Our method detects obstacles within the drivable area, as these are the ones posing a danger to the ve-



Method	Model-variant	Fishyscapes: Lost & Found		Road Obstacles	
		AP $\uparrow$	FPR <sub>95</sub> $\downarrow$	AP $\uparrow$	FPR <sub>95</sub> $\downarrow$
Ours	big object training	<b>84.4</b>	<b>5.2</b>	<b>86.1</b>	2.7
	standard object training	81.0	9.1	75.9	15.8
Discriminative Outlier Detection Head [2]	combined probability	68.3	10.7	68.1	19.1
	random sized patches	60.9	27.0	70.6	<b>1.0</b>
	fixed sized patches	50.0	73.9	31.4	28.1
Resynthesis [21]	discrepancy network	65.4	6.9	43.7	2.3
Dirichlet DeepLab [22]	prior entropy	61.1	70.8	10.7	22.8
Learned Embedding	minimum NLL	60.3	8.5	2.1	31.3
Density [4]	logistic regression	55.3	9.0	1.8	33.9
	single-layer NLL	47.5	17.3	-	-
Bayesian DeepLab [23]	entropy	53.7	37.3	-	-
	mutual information	43.6	34.0	8.2	57.9
DeepLab Softmax [19]	entropy	29.2	41.0	16.1	9.1
kNN Embedding	density	21.8	20.9	-	-
	relative class density	6.9	100.0	-	-
OoD training	void classifier	14.9	24.2	9.3	48.8
	max-entropy	13.6	14.1	2.4	11.6

Table 4. **Obstacle detection scores.** The primary metric is *average precision* of detecting obstacle pixels. The new entry *Ours - big object training* denotes a variant of our method which was trained with a wider range of synthetic obstacle sizes. This change improves both metrics, with a remarkable effect on FPR<sub>95</sub>.

hicle. Our approach can work with any source that provides drivable area information.

In our experiments, we use the PSP-Net semantic segmentation network of [38] trained on the Cityscapes dataset [6], as implemented in the framework of [9]. We take the road area to be all pixels classified as either *road* or *sidewalk*, since the diverse road textures we are targeting can be classified as either. Note that standard categories, such as *car* and *pedestrian*, are inherently accounted for by PSP-Net; we then focus on the unusual obstacles for which *no* training data, neither supervised not unsupervised, is available. Nevertheless, since such unusual obstacles could be partially classified as non-road, we include the regions containing other classes that are fully enclosed within the road area. Examples outputs of the process are shown in Fig. 10.

## B.2. Discrepancy Network Architecture

We use the discrepancy network architecture of [21] but without the semantic branch, since we aim for compatibility with non-semantic free-space estimation methods. The architecture is shown in Fig. 13.

The network has two input streams: the original image and the image where the road area has been inpainted. We apply Gaussian blur to the input image to eliminate excessive high-frequency signals, as described in the main article. We use the pretrained VGG network of [30] to extract features from both images. At four levels of the feature pyramid, we fuse the

two streams of features in these two parallel ways:

- Concatenate stream 1 and 2, followed by a  $1 \times 1$  convolution,
- Calculate pixel-wise correlation of features, following [20].

The results of the above are concatenated and passed on to an up-convolution pyramid which uses the SeLU [17] activation function. In the final step, the discrepancy score is multiplied by the binary drivable space mask, since the outputs are only valid within the road area.

## B.3. Discrepancy Network Training

The discrepancy network was trained for 65 epochs. Each epoch iterates over the 2975 frames of our synthetic training set. The training is done using  $768 \times 384$  crops of the road area. To improve training reproducibility, we pre-define the crops and their ordering in each epoch, and train all variants of the discrepancy network with the same sequence of samples.

We use binary cross entropy loss, but due to strong class imbalance between obstacles and background, the obstacle pixels’ loss contribution are weighted higher than those of background pixels. We maintain the weights set as in [21].

We use the Adam [16] optimizer. We set the initial learning rate to  $10^{-4}$  and then adjust it dynamically, if there is no improvement of validation loss for 5 consecutive epochs, the learning rate is reduced 10 times. We

generate the validation set from Cityscapes validation subset in the same way as the training set.

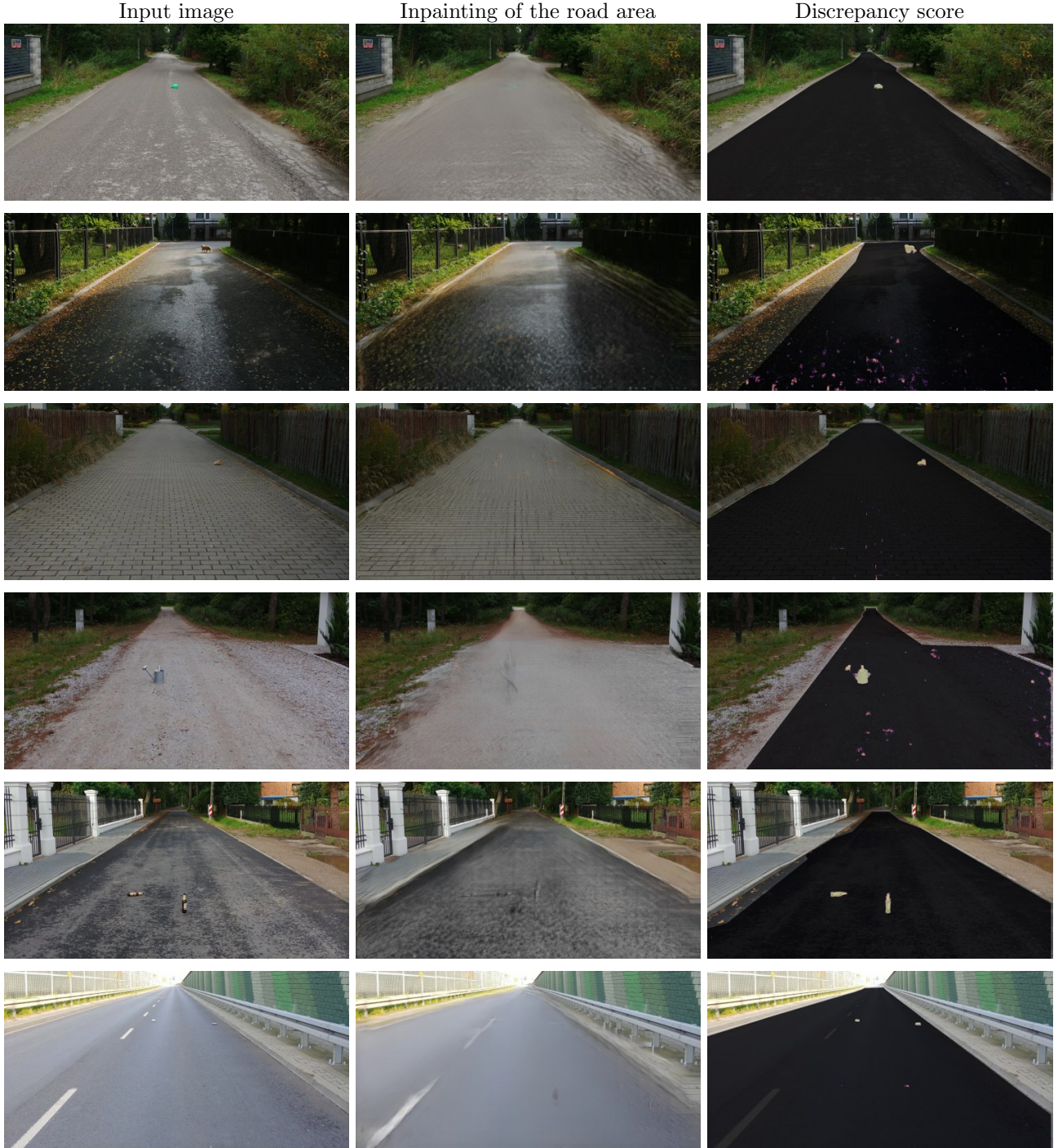


Figure 11. **Example outputs of our method for the Road Obstacles dataset.** **Left:** Input images featuring challenging or distant obstacles. **Center:** The result of sliding-window inpainting of the road area. **Right:** The discrepancy score calculated by our network given the two previous images. The darkened area corresponds to the ground-truth drivable space.



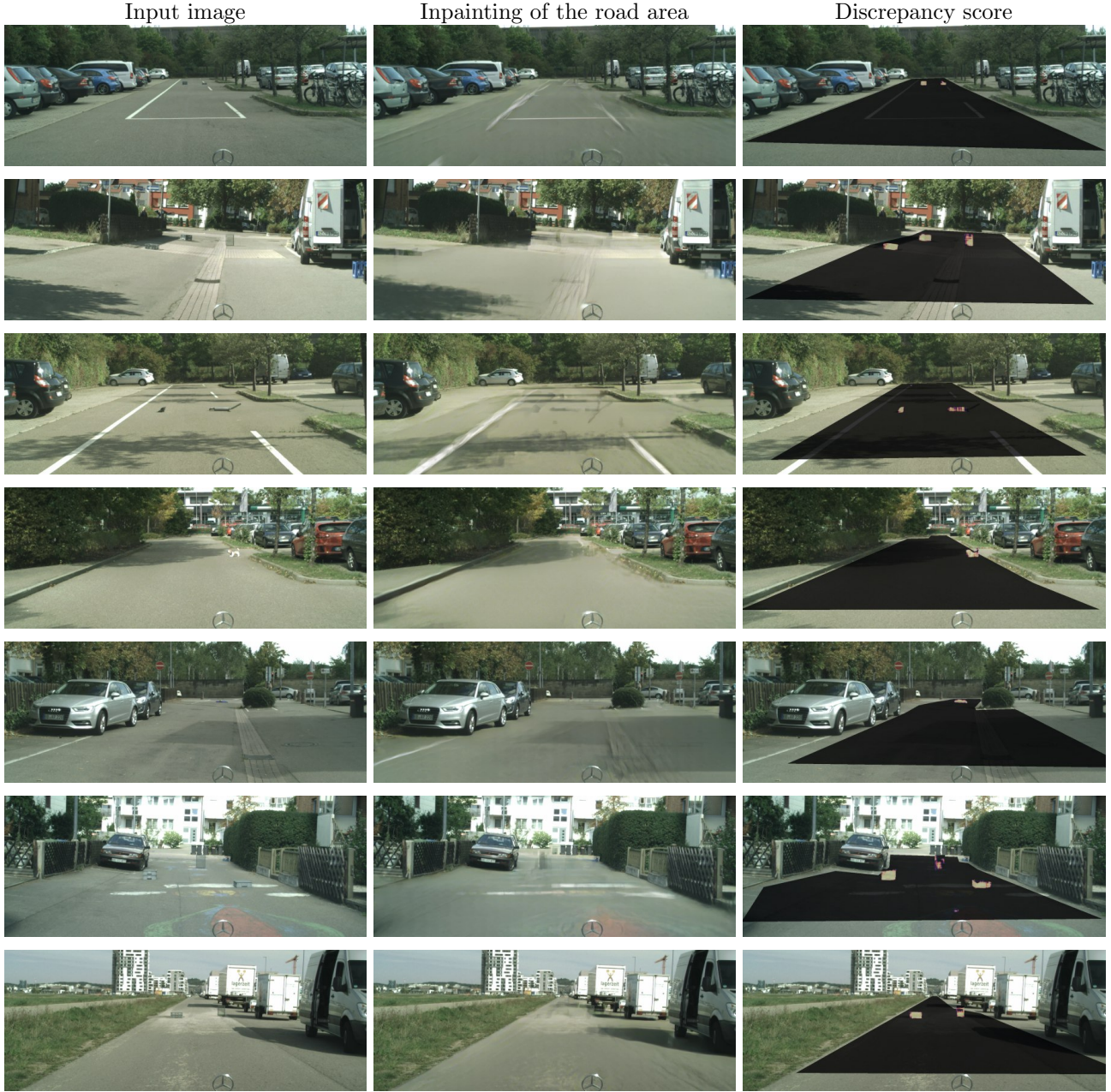


Figure 12. **Example outputs of our method for the Fishyscapes Lost & Found dataset. Left:** Input images; some of the non-drivable area has been cropped for easier viewing. **Center:** The result of sliding-window inpainting of the road area. **Right:** The discrepancy score calculated by our network given the two previous images. The darkened area corresponds to the ground-truth drivable space.

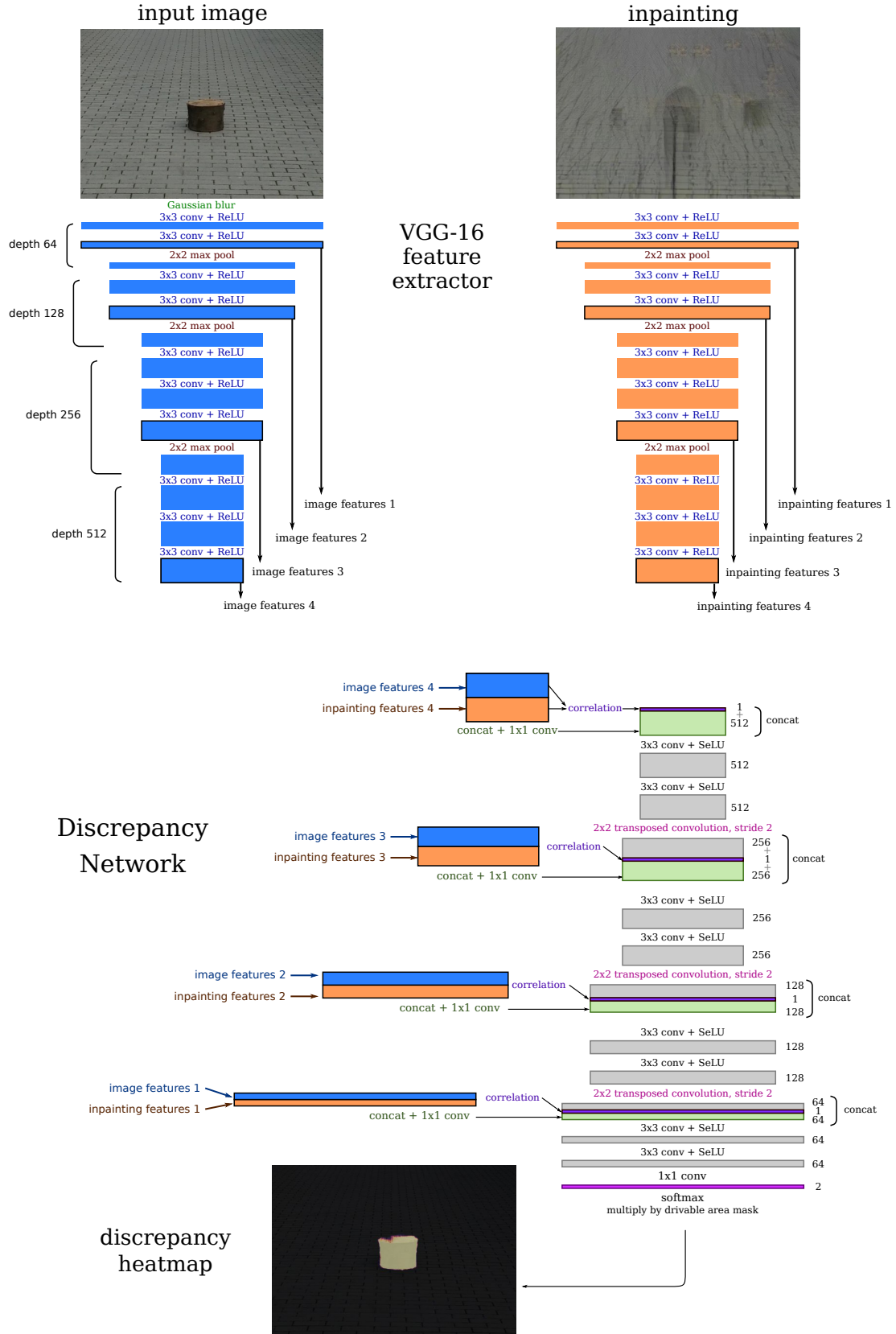


Figure 13. Discrepancy network architecture.

